

# No X-Ray Excess from the HESS J1741–302 Region except a New Intermediate Polar Candidate

Hideki UCHIYAMA,<sup>1</sup> Katsuji KOYAMA,<sup>2</sup> Hironori MATSUMOTO,<sup>3</sup> Omar TIBOLLA,<sup>4,5</sup> Sarah  
KAUFMANN,<sup>6</sup>

and Stefan WAGNER<sup>6</sup>

<sup>1</sup>*Department of Physics, School of Science, The University of Tokyo, 7-3-1 Hongo, Bunkyo-ku,  
Tokyo 113-0033*

*uchiyama@juno.phys.s.u-tokyo.ac.jp*

<sup>2</sup>*Department of Physics, Graduate school of Science, Kyoto University, Oiwake-cho, Kitashirakawa,  
Kyoto 606-8502*

*koyama@cr.scphy.kyoto-u.ac.jp*

<sup>3</sup>*Kobayashi-Maskawa Institute for the Origin of Particles and the Universe, Nagoya University,  
Furo-cho, Chikusa-ku, Nagoya, 464-8601*

<sup>4</sup>*Max-Planck-Institut für Kernphysik, P.O. Box 103980, D96029 Heidelberg, Germany*

<sup>5</sup>*Universität Würzburg, 97074 Würzburg, Germany*

<sup>6</sup>*Landessternwarte, Universität Heidelberg, Königstuhl, D 69117 Heidelberg, Germany*

(Received ; accepted )

## Abstract

With the Suzaku satellite, we observed an unidentified TeV gamma-ray source HESS J1741–302 and its surroundings. No diffuse or point-like X-ray sources are detected from the bright southern emission peak of HESS J1741–302. From its neighborhood, we found a new intermediate polar candidate at the position of  $(\alpha, \delta)_{J2000.0} = (17^{\text{h}}40^{\text{m}}35^{\text{s}}.6, -30^{\circ}14^{\text{m}}16^{\text{s}})$ , which is designated as Suzaku J174035.6–301416. The spectrum of Suzaku J174035.6–301416 exhibits emission lines at the energy of 6.4, 6.7 and 7.0 keV, which can be assigned as the  $K\alpha$  lines from neutral, He-like and H-like iron, respectively. A coherent pulsation is found at a period of  $432.1 \pm 0.1$  s. The pulse profile is quasi-sinusoidal in the hard X-ray band (4–8 keV), but is more complicated in the soft X-ray band (1–3 keV). The moderate period of pulsation, the energy flux, and the presence of the iron  $K\alpha$  lines indicate that Suzaku J174035.6–301416 is likely an intermediate polar, a subclass of magnetized white dwarf binaries (cataclysmic variables). Based on these discoveries, we give some implications on the origin of GCDX and brief comments on HESS J1741–302 and PSR B1737–30.

**Key words:** Galaxy: Center—Magnetic Cataclysmic Variable —Intermediate

## 1. Introduction

The most characteristic feature of the Galactic center (GC) region in the high energy band is the Galactic center diffuse X-ray emission (GCDX). It has strong emission lines at 6.4, 6.7 and 7.0 keV which are  $K\alpha$  lines from neutral, He-like and H-like Fe ions, respectively (e.g. Koyama et al. 2007b). Chandra (Muno et al. 2003; Muno et al. 2009) resolved the GCDX into many faint X-ray sources. The integrated spectra of the point sources resemble the GCDX in the  $K\alpha$  line features (Muno et al. 2004, Koyama et al. 2007b). The most probable candidates responsible for the  $K\alpha$  lines are magnetic cataclysmic variables (mCVs) and/or active stars (Muno et al. 2004; Revnivtsev et al. 2009). Therefore, a significant fraction of the GCDX, if not all, is due to these X-ray point sources. In fact, Chandra, XMM-Newton and Suzaku have already found several point sources which exhibit characteristic properties of mCVs such as moderate pulse periods and X-ray spectra with the prominent iron  $K\alpha$  lines (e.g. Nobukawa et al. 2009). The equivalent widths of the  $K\alpha$  lines are smaller than those in the GCDX, and hence the origin of the GCDX is still debatable.

The H.E.S.S. Cherenkov telescope revealed that TeV gamma-ray sources (Aharonian et al. 2006a) and the large-scale diffuse TeV gamma-ray emission (Aharonian et al. 2006b) are also present in the GC region. The most plausible scenario of the origin of the TeV gamma-rays is interaction of molecular cloud with TeV energy protons (high-energy cosmic rays). The cosmic ray must contain a large number of lower-energy proton, which may produce a  $K\alpha$  line of neutral iron (the 6.4 keV line) by the inner-shell ionization of the iron atoms in the molecular cloud. Accordingly, it is conceivable that the TeV gamma-ray emission is associated with the 6.4 keV line. In fact, Bamba et al. (2009) reported possible association of TeV gamma-ray source HESS J1745–303 with the 6.4 keV line.

HESS J1741–302 (Tibolla et al. 2009a; Tibolla et al. 2009b) is one of the faintest unidentified TeV gamma-ray sources. It is located near a relatively powerful radio pulsar PSR B1737–30 with the spin-down luminosity of  $\sim 8 \times 10^{33}$  erg s<sup>−1</sup> (Fomalont et al. 1997). In order to search for possible connection between the TeV gamma-ray emission and the 6.4 keV line, we observed the region of HESS J1741–302 with the Suzaku satellite twice. We found no X-ray excess from the bright southern emission peak of HESS J1741–302 nor PSR B1737–30. Instead, we discovered a new probable mCV at the close vicinity of PSR B1737–30.

This paper focuses on the discovery and property of the new mCV candidate, and some implications on the origin of GCDX. We also give brief comments on the non-detection of X-ray from HESS J1741–302 and PSR B1737–30.

**Table 1.** Suzaku observation data list.

Target	Obs. ID	Start Time (UT)	Stop Time (UT)	Good Exposure Time (ks)*
GC LARGEPROJECT15	503021010	2008-10-04 03:44:03	2008-10-05 10:57:24	50.1
HESSJ1741-B	503077010	2009-02-26 01:00:60	2009-02-27 11:35:19	46.2

\* After the data screening described in the text.

## 2. Observations and Data Reduction

The Suzaku X-ray Imaging Spectrometer (XIS) observed the regions near the radio pulsar PSR B1737–30 (Fomalont et al. 1997) and HESS J1741–302 (Tibolla et al. 2009a; Tibolla et al. 2009b) twice; one was as the Suzaku deep survey project of the Galactic center region and the other was the pointing observation on the unidentified TeV gamma-ray source HESS J1741–302. Details about these observations are listed in table 1.

The XIS consists of four sets of X-ray CCD camera systems (XIS 0, 1, 2, and 3) placed on the focal planes of four X-Ray Telescopes (XRT) aboard the Suzaku satellite. XIS 0, 2, and 3 have front-illuminated (FI) CCDs, while XIS 1 has a back-illuminated (BI) CCD. One of the FI CCD cameras (XIS 2) has been out of function since November 2006, and hence the data of XIS 2 have not been used. Detailed descriptions of the Suzaku satellite, the XRT, and the XIS can be found in Mitsuda et al. (2007), Serlemitsos et al. (2007), and Koyama et al. (2007a).

The XIS observations were made with the normal mode. The CCD integration time is 8 s in this mode. We used the cleaned XIS event data distributed from DARTS<sup>1</sup>. These cleaned data were processed with the processing version 2.2.11.22 and 2.2.11.24 for the first and second observations, respectively. The difference of the processing versions has no significant effect on the results.

In these processes, the data during the epoch of low Earth elevation angles less than 5 degrees ( $\text{ELV} < 5^\circ$ ), day Earth elevation angles less than 20 degrees ( $\text{DYE\_ELV} < 20^\circ$ ), and within the South Atlantic Anomaly were removed. The good exposure times are listed in table 1. Although the XIS CCDs were significantly degraded by on-orbit particle radiation, the CCD performances were restored by the spaced-row charge injection technique (Prigozhin et al. 2008; Uchiyama et al. 2009). Using on board calibration sources, we confirmed the spectral resolutions at 5.9 keV were  $\sim 150$  and  $\sim 200$  eV (FWHM) for the FI and BI CCDs, respectively.

Due to a star tracker (STT) problem, the Suzaku attitude during the second observation was not locked at the programmed position, and hence drifted by  $\sim 2'$  in the direction of the right ascension between the start and stop time of the second observation. The second observation data therefore were not used for the detailed imaging analysis (section 3.1) but were used for

<sup>1</sup> <http://www.darts.isas.jaxa.jp/astro/suzaku>.

the spectral and timing analysis (section 3.2 and 3.4) after the position correction as described in section 3.2.

### 3. Analysis and Results

We analyzed the data using the software package HEASoft 6.5.1. In this paper, uncertainties are quoted at the 90% confidence range unless otherwise stated.

#### 3.1. X-ray Image

To make X-ray images, we used only the data of October 2008 when the STT operated correctly. To increase statistics, the data of XIS 0, 1 and 3 were merged. Since the intensity of the non-X-ray background (NXB) depends on the geomagnetic cut-off rigidity (COR) (Tawa et al. 2008), we obtained COR-sorted NXB images using `xisnxbgen`. After subtracting the NXB image, we divided the X-ray image by a flat-field image to correct vignetting. The flat-field image was made with `xiessim` (Ishisaki et al. 2007).

Since Suzaku has non-negligible position errors (Uchiyama et al. 2008), we fine-tuned the coordinate of the XIS image using the positions of catalogued visible stars. Since X-rays from normal stars are generally soft, we made a 0.5–2.0 keV band image. In the X-ray image, there are three point sources which correspond to catalogued infrared and visible stars, whose positional errors are less than 0".1 (Cutri et al. 2003; Hog et al. 1998). To match the positions of the three stars, we simply shifted and rotated the Suzaku coordinate without any stretch or shear of the original Suzaku image. The result is shown in figure 1. After this fine-tuning, the averaged difference between the catalogued stars and the Suzaku position is 9". We regard this value as the systematic error. We then constructed the 1–9 keV band image from the first observation (figure 2), in which the NXB was subtracted and the vignetting was corrected in the same way as figure 1.

No significant X-ray emission is found from the radio pulsar PSR B1737–30, but a bright new source is discovered at about 90" east of PSR B1737–30 with the fine-tuned position of  $(\alpha, \delta)_{2000} = (17^{\text{h}}40^{\text{m}}35^{\text{s}}.6, -30^{\circ}14^{\text{m}}16^{\text{s}})$ . Here we designated this source as Suzaku J174035.6–301416. The uncertainties are 11" and 9" due to statistical and systematic errors, respectively. Thus overall uncertainty is evaluated as 14".

Near Suzaku J174035.6-301416, we found two catalogued sources, SAX J1740.5-3013 (Huovelin et al. 1999) and AX J1740.5-3014 (Sakano et al. 2002). The offset from Suzaku J174035.6-301416 and error radius of SAX J1740.5-3013 are 62" and about 50", respectively, while those of AX J1740.5-3014 are 107" and about 90". With the error radius of Suzaku J174035.6-301416 of 14", the error regions of the three objects overlap with each others, and hence could be the same source. These sources were also observed by Parmar et al. (2003) with the INTEGRAL satellite, but were not detected due to the larger detection limit than that of Suzaku.

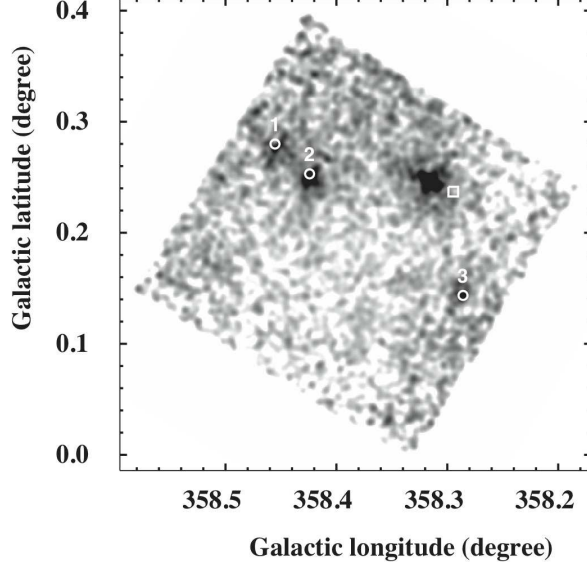


**Fig. 1.** X-ray image in the 0.5–2 keV band after the coordinate correction (see text in section 3.1). The numbered circles represent catalogued stars used as references of the position. (1) DENIS-P J174047.6–300613 (2) HD 316162 (3) DENIS-P J174054.9–301915 (Cutri et al. 2003; Hog et al. 1998). The rectangle mark shows the position of PSR B1737–30 (Fomalont et al. 1997). The NXB was subtracted and the vignetting was corrected (see text). This image was smoothed using a Gaussian function with  $\sigma = 0'.35$ .

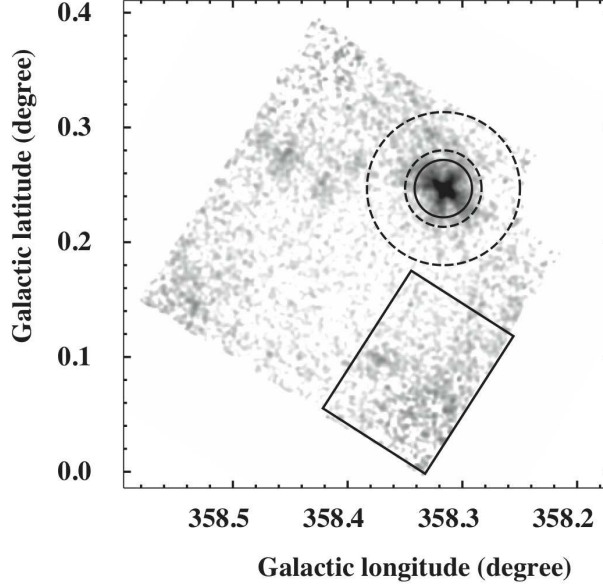


**Fig. 2.** X-ray image in the 1–9 keV band after the coordinate correction. The source and background regions for spectra and light curves of Suzaku J174035.6–301416 are shown by the solid circle and dashed annulus, respectively. The solid box shows the source region of HESS J1741–302. The NXB was subtracted and the vignetting was corrected in the same way as figure 1. This image was smoothed using a Gaussian function with  $\sigma = 0'.2$ .

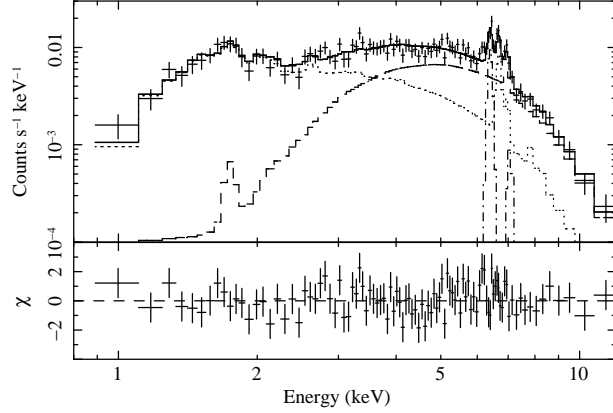


**Fig. 3.** Background-subtracted spectrum of Suzaku J174035.6–301416 for the FI CCDs. The source spectrum was extracted from the solid circle in figures 2, while the local background spectrum was taken from the dashed annulus described in figure 2. The vertical error bars of the each data point are the  $1\sigma$  error. The solid line is the best-fit result of the two-components CIE model shown in table 2(b). The dashed and dotted lines represent the high- and low-temperature CIE components. The dash-dot lines represent the neutral iron  $K\alpha$  and  $\beta$  lines. Although the fitting was made simultaneously for the FI and BI spectra, only the FI result is given for simplicity

### 3.2. Spectrum of Suzaku J174035.6–301416

The spectra of Suzaku J174035.6–301416 were extracted from the solid circle region with a radius of  $1'.5$  and subtracted by the background spectra evaluated in the near region described by the dashed annulus with radii of  $2'$  and  $4'$  shown in figure 2.

In the second observation, however, the STT was troubled and the position drifted slowly. We therefore divided the data of the second observation into six data sets. In the each data set, the attitude drift is less than  $20''$ , which is comparable to the positional uncertainty of  $14''$ . We made X-ray images from these six data sets respectively and decided the peak positions of Suzaku J174035.6–301416 in the each data. We corrected the coordinates of the six data sets to match the peak positions with each others. Then we made positional fine tuning with the same method as section 3.1. After these corrections, the spectra and light curves (section 3.3) for the second observation were extracted.

The difference between the fluxes of the first and second observations are less than 5 % and we did not find clear difference between the shapes of the spectra. We thus combined the spectra of XIS of the both observations to increase the statistics. The spectra of the two FIs (XIS 0, 3) were co-added because the response functions are almost the same between the FIs. The X-ray spectrum is shown in figure 3, where only the spectrum of the FI CCDs is given for simplicity. XIS response and XRT auxiliary files were made using `xismfgen` and `xissimarfgen` (Ishisaki et al. 2007) for the each observation. These response and auxiliary files were also combined.

The X-ray spectra exhibit three lines at 6.4, 6.7, and 7.0 keV. In order to identify these



lines, the spectra were fit with a phenomenological model of an absorbed power-law plus three narrow Gaussian lines in the 5–10 keV band. The cross section of the photoelectric absorption was obtained from Morrison & McCammon (1983). The best-fit line energies of these three lines are  $6.40^{+0.04}_{-0.02}$  keV,  $6.67 \pm 0.02$  keV and  $6.95^{+0.04}_{-0.05}$  keV, while the equivalent widths (EW) are  $210^{+30}_{-50}$  eV,  $190^{+60}_{-40}$  eV and  $130^{+40}_{-50}$  eV, respectively. From the line energies, these are identified as the  $K\alpha$  lines from neutral, He-like and H-like iron.

We fitted the X-ray spectra of the FI and BI simultaneously with a one-component collisional ionization equilibrium (CIE) plasma model (APEC: Smith et al. 2001). We added two Gaussians, FeI  $K\alpha$  (6.40 keV) and FeI  $K\beta$  (7.06 keV). The energy of FeI  $K\beta$  is near to FeXXVI  $K\alpha$ , and hence was not separable. In order to estimate the FeXXVI  $K\alpha$  emission accurately, we included the FeI  $K\beta$  (7.06 keV). According to Kaastra & Mewe (1993), the ratios of the center energies and line flux for the neutral iron  $K\alpha$  and  $K\beta$  lines were fixed to be 1:1.103 and 1:0.125, respectively. The abundance of the CIE plasma model was free but the relative ratio among elements was fixed to be the solar value (Anders & Grevesse 1989). This model is rejected with  $\chi^2/\text{d.o.f.} = 363.3/166$ . The same model but two-components CIE plasma with the common absorption and abundance is also rejected with  $\chi^2/\text{d.o.f.} = 275.7/164$ .

Since large residuals are found in the low energy band, we applied a one-component CIE plasma with partial absorption model. This model gives a marginal  $\chi^2/\text{d.o.f.}$  of 204.9/164. The best-fit parameters are listed in table 2(a).

We finally tried a two-components CIE plasma with the independent absorptions and common abundance model, and obtained the most reasonable fit with  $\chi^2/\text{d.o.f.} = 190.6/163$ . The best-fit parameters and the result are shown in table 2(b) and figure 3.

### 3.3. X-ray limits from PSR B1737–30 and HESS J1741–302

Although the detailed morphology of HESS J1741–302 may not be final (Tibolla et al. 2009a; Tibolla et al. 2009b), the global size and the peak position are reliable. HESS J1741–302 consists of southern and northern bright hot spots, whose sizes are  $\sim 0.1$  and  $\sim 0.2$  (FWHM) (Tibolla et al. 2009b). The former spot corresponds to the south west corner of the Suzaku field (the lower corner in figure 2). Compared to the other region in figure 2, we see no excess X-rays from this region in the 1–9 keV band. Also no X-rays are found from the position of PSR B1737–30 (the rectangle in figure 1).

In order to estimate the upper limit of the fluxes, we extract the spectrum from the southern TeV gamma-ray emission peak region of HESS J1741–302, the solid box ( $6' \times 9'$ ) in figure 2. The background was taken from the remaining region of the XIS field excluding the  $4'$ -radius circle region around Suzaku J174035.6–301416. The background subtracted spectrum was fit with an absorbed power-law. The photon index was fixed to 2.0, the typical value of pulsar wind nebula, while the absorption column was assumed to be the same as Suzaku J174035.6–301416,  $N_{\text{H}} = 1.6 \times 10^{22} \text{ cm}^{-2}$ . Then the flux upper limit was evaluated to

**Table 2.** Best-fit parameters of the model fittings for the background-subtracted spectra\*.

(a) one-component CIE plasma with partial absorption model		
Model: $\text{Abs}[1] \times \{(1-\alpha) + \alpha \times \text{Abs}[2]\} \times (\text{APEC} + \text{Neutral Iron Lines})$		
Iron Lines	Fe I $K\alpha$	Fe I $K\beta$
Energy (keV)	$6.40^{+0.03}_{-0.02}$	$7.06^\dagger$
Flux ( $10^{-6}$ ph s $^{-1}$ cm $^{-2}$ )	$8.8^{+1.7}_{-1.3}$	$1.1^\dagger$
Parameter	APEC	
$kT$ (keV)	$9.5^{+1.2}_{-0.9}$	
Abundance (solar)	$0.49^{+0.11}_{-0.10}$	
Normalization $^\ddagger$	$2.8^{+0.1}_{-0.2}$	
Parameter	Abs[1]	Abs[2]
$N_{\text{H}}$ ( $10^{22}$ cm $^{-2}$ )	$1.7^{+0.1}_{-0.2}$	$16 \pm 3$
Covering factor $\alpha$	—	$0.71^{+0.02}_{-0.03}$
Flux ( $10^{-12}$ erg s $^{-1}$ cm $^{-2}$ ) $^\S$	2.0 (2.2)	
$\chi^2/\text{d.o.f.} = 204.9/164$		
(b) two-components CIE plasma model		
Model: $\text{Abs}[1] \times (\text{APEC}[1] + \text{Neutral iron lines}) + \text{Abs}[2] \times \text{APEC}[2]$		
Iron Lines	Fe I $K\alpha$	Fe I $K\beta$
Energy (keV)	$6.40^{+0.03}_{-0.02}$	$7.06^\dagger$
Flux ( $10^{-6}$ ph s $^{-1}$ cm $^{-2}$ )	$8.4^{+1.7}_{-1.4}$	$1.0^\dagger$
Parameter	APEC[1]	APEC[2]
$kT$ (keV)	$64(\geq 44)$	$6.0 \pm 1.1$
Abundance (solar) $^\parallel$	$1.3^{+0.2}_{-0.3}$	
Normalization $^\ddagger$	$1.6^{+0.2}_{-0.1}$	$0.62^{+0.04}_{-0.03}$
Parameter	Abs[1]	Abs[2]
$N_{\text{H}}$ ( $10^{22}$ cm $^{-2}$ )	$11^{+2}_{-1}$	$1.6 \pm 0.1$
Flux ( $10^{-12}$ erg s $^{-1}$ cm $^{-2}$ ) $^\S$	2.1 (2.3)	
$\chi^2/\text{d.o.f.} = 190.6/163$		

\* Errors show 90% confidence range.

 $^\dagger$  The energy and flux of Fe I  $K\beta$  line are fixed to be 1.103 and 0.125 times of those of Fe I  $K\alpha$  line, respectively. $^\ddagger$  The units of  $10^{-17}/(4\pi D^2) \int n_e n_H dV$ , where  $D$ ,  $n_e$  and  $n_H$  are the distance to the source (cm), the electron density (cm $^{-3}$ ), and the hydrogen density (cm $^{-3}$ ), respectively. $^\S$  Observed flux in the range of 2–10 keV. The values in parentheses are corrected with the absorption  $N_H = 1.7 \times 10^{22}$  cm $^{-2}$  (a) or  $1.6 \times 10^{22}$  cm $^{-2}$  (b) as the interstellar absorptions. $^\parallel$  The abundances are common between APEC[1] and APEC[2] in (b).



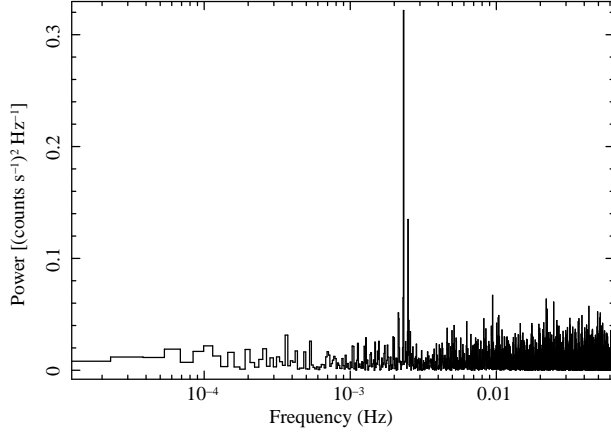


**Fig. 4.** Power spectrum (FFT) in the 1–9 keV band.

be  $< 1.6 \times 10^{-13} \text{ erg s}^{-1} \text{ cm}^{-2}$  in the 90% confidence level.

With the same method, we estimated the X-ray upper-limit of PSR B1737–30 in the 1′-radius circle excluding the 1′5-radius circle region around Suzaku J174035.6–301416. For the background, we used the same background region above. Since the half power diameter of the XRT is  $\sim 2'$ , the spectrum from the region including PSR B1737–30 is contaminated by Suzaku J174035.6–301416. Using the XIS simulator *xissim* (Ishisaki et al. 2007), we calculated the contaminating flux to be 16% of Suzaku J174035.6–301416. After subtraction of this contamination, the spectrum from the region including PSR B1737–30 was fitted with the same model above. Then we evaluated the flux upper limit to be  $< 3.5 \times 10^{-13} \text{ erg s}^{-1} \text{ cm}^{-2}$  in the 90% confidence level.

The flux upper limit from the former large region ( $6' \times 9'$ ) is smaller than that for the region including PSR B1737–30, which is assumed to be a point source. It seems a little strange. The later region is, however, small and the photon statistics are low. On the other hand, the contamination from Suzaku J174035.6–301416 is quite high. Thus the upper limit becomes large.

#### 3.4. Timing analysis of Suzaku J174035.6–301416

We searched for a coherent pulsation in the 1–9 keV band from the FI data of the both observations. We did not use the BI data because it had high and time-variable NXB, especially above the 7 keV band. The fast Fourier transform (FFT) analysis revealed a clear peak at  $\sim 2.3 \times 10^{-3} \text{ Hz}$  as is shown in figure 4. We then searched for an accurate pulse period with the folding technique, and found a pulse period of  $432.1 \pm 0.1 \text{ s}$ . The error of the pulse period was estimated with the method given in Larsson (1996).

The sub-peak at  $2.5 \times 10^{-3} \text{ Hz}$  in figure 4 would be the beat frequency between the 432.1-s period and the Suzaku orbital period of about 96 minutes.

Since we found the two-components CIE plasma in the spectral analysis, we made folded

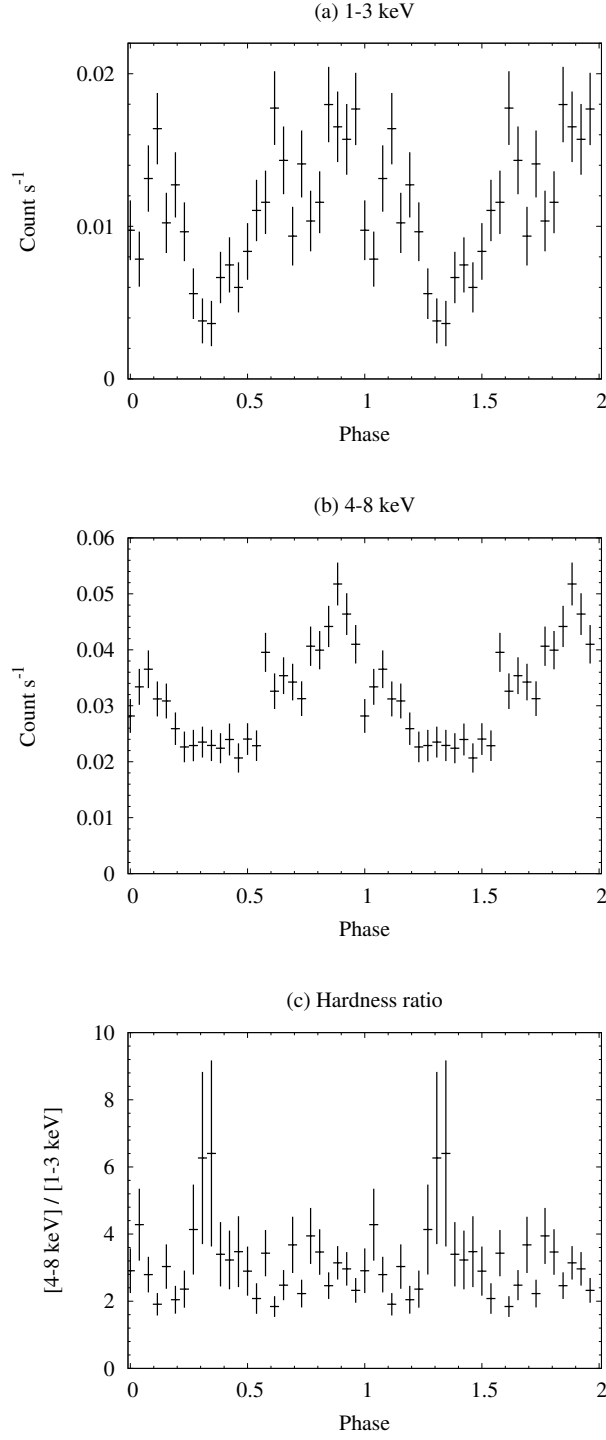


**Fig. 5.** (a) Pulse profile in the 1–3 keV band, (b) that of the 4–8 keV band. The count rates of the background region are subtracted. (c) Hardness ratio of the 4–8 keV to 1–3 keV. Folded period is 432.1 s. The vertical error bars of each data point are the  $1\sigma$  error.

pulse profiles in the 1–3 keV and 4–8 keV bands representing the low- and high-temperature components, respectively. These folded pulse profiles are shown in figure 5, where normalized count rates of the background region,  $4.7 \times 10^{-3}$  (1–3 keV) and  $6.2 \times 10^{-3}$  (4–8 keV) counts  $\text{s}^{-1}$ , were subtracted. We also show the hardness ratio between these bands. The pulse profiles appear to be different between the two components. The pulse profile of the high-temperature plasma is quasi-sinusoidal with small humps in the both sides of the main peak, while that of the low-temperature plasma is more complicated with nearly equal three peaks. The minima are deeper, but narrower, in the soft band compared to the hard band. The former is expected if  $N_{\text{H}}$  is varying as is common in intermediate polars (IPs) (Norton & Watson 1989).

## 4. Discussion

### 4.1. Nature of *Suzaku* J174035.6–301416

The fine-tuned position of *Suzaku* J174035.6–301416 at  $(\alpha, \delta)_{2000} = (17^{\text{h}}40^{\text{m}}35^{\text{s}}.6, -30^{\circ}14^{\text{m}}16^{\text{s}})$  is different from that of PSR B1737–30 at  $(\alpha, \delta)_{2000} = (17^{\text{h}}40^{\text{m}}33^{\text{s}}.82, -30^{\circ}15^{\text{m}}43^{\text{s}}.5)$  (Fomalont et al. 1997). The X-ray spectra of *Suzaku* J174035.6–301416 exhibit  $\text{K}\alpha$  lines at 6.4, 6.7, and 7.0 keV with the best-fit EW values of  $\sim 210$ ,  $\sim 190$ , and  $\sim 130$  eV, respectively. These EW values are nearly the same as the mean EW of mCVs (Ezuka & Ishida 1999), which are  $\sim 100$ ,  $\sim 200$ , and  $\sim 100$  eV. We found a coherent and clear pulsation of 432.1 s from *Suzaku* J174035.6–301416. This is usual spin period of mCVs, which typically ranges from 30 s to  $2 \times 10^4$  s (Scaringi et al. 2010). Although we found no periodicity due to orbital modulation of *Suzaku* J174035.6–301416, this 432.1-s period would be due to spin, because this value is smaller than typical orbital period, which ranges from 2 to 10 hours (Scaringi et al. 2010).

As shown in section 3.1, *Suzaku* J174035.6–301416 is likely to be identical to AX J1740.5–3014 and SAX J1740.5–3013. The latter two sources were observed in September 1995 and in April 1998, respectively. The data qualities of these sources, however, were too limited to perform spectral and timing analysis. Nevertheless, Sakano et al. (2002) and Huovelin et al. (2002) reported the fluxes of these sources are 2.5, and  $2.4 \times 10^{-12}$   $\text{erg s}^{-1} \text{cm}^{-2}$ , respectively. Since the *Suzaku* flux is  $2.1 \times 10^{-12}$   $\text{erg s}^{-1} \text{cm}^{-2}$ , we see no large variability in the long time span of  $\sim 10$  years.

The overall spectrum of *Suzaku* J174035.6–30141 was well fit with the two-components CIE plasma with temperatures of 6.0 and 64 keV or marginally fit with the one-component CIE plasma with partial covering. The both models require the  $\text{K}\alpha$  (6.40 keV) from neutral iron. Ezuka and Ishida (1999) also reported that the spectra of mCVs can be described by a thin thermal plasma model with a mean temperature of  $\sim 20$  keV plus 6.4 keV line. The one-component CIE plasma with partial covering model gives a temperature of 10 keV, which resembles to the general feature of mCVs. We however favor the two-components CIE plasma

model, because  $\chi^2$  is better and the energy dependent pulse profile is difficult to explain with the one-component CIE plasma model.

The slow pulsation and X-ray spectrum, in particular the iron  $K\alpha$  line features suggest that Suzaku J174035.6–301416 is a new persistent mCV. It is more likely to be an IP and not a polar, because the 432.1-s period is too short as a synchronized orbital-spin period ( $\geq 4000$  s for all the catalogued polars by Ritter & Kolb 2003). The lack of long term variability in the X-ray flux of this IP candidate is indeed typical of this class, as they do not show off states, and only have very short dwarf nova-type outbursts. For the definitive classification, the optical spectrum and light curve of Suzaku J174035.6–301416 are required. Using the SIMBAD database<sup>2</sup>, we searched a corresponding object but there is no catalogued optical object within  $80''$  around Suzaku J174035.6–301416.

We suggest that a large absorption for the 64 keV plasma is due to the circum-stellar gas, which could be up to a few  $\times 10^{23}$  cm<sup>-2</sup> (Ezuka & Ishida 1999). This large amount of circum-stellar gas can naturally explain the origin of the strong 6.4 keV line from neutral iron (see e.g. Ezuka & Ishida 1999).

The spectrum of the standard model with a cylindrical emission region is given by multi-temperature plasma components with power-law emission measure distribution of index  $\sim -0.5$  (Ishida et al. 1994). The multi-components plasma can be approximated by two representative temperatures. The ratio of the volume emission measures of the 6.0 keV plasma to the 64 keV plasma is 1:2.6. This ratio does not follow the power-law relation of  $\sim -0.5$ . It is also strange that the 6.0 keV plasma emission does not suffer the large absorption, if that is attributable to the circum-stellar gas. This new IP seems difficult to be explained with the standard emission model and geometry. However, the spectra of IPs are complex with multi-temperatures, soft blackbody components (e.g. Evans & Hellier 2007) and hard reflection components (e.g. Revnivtsev et al. 2004) so on. In addition, the spectra depend strongly on spin and orbital phase (e.g. Allan et al. 1998). Our spectral model is unlikely to be a unique description. The statistic of this source is, however, not so high, and the detail modeling is beyond the scope of this paper.

The absorption for the low temperature component, on the other hand, can be inter-stellar medium to Suzaku J174035.6–301416. The typical absorption to the GC region is  $N_H = 6 \times 10^{22}$  cm<sup>-2</sup> (e.g. Sakano et al. 2002, Ryu et al. 2009). However this value rapidly decreases as one moves away from the Galactic Plane. For example, G359.1–0.5, a GC supernova remnant located  $0.3$ – $0.5$  away from the plane, has absorption of about  $N_H = 2 \times 10^{22}$  cm<sup>-2</sup> (Ohnishi et al. 2010). Suzaku J174035.6–301416 has  $N_H = 1.6 \times 10^{22}$  cm<sup>-2</sup>, nearly identical to G359.1–0.5, and hence might be a GC source. Assuming the distance to GC as 8 kpc (e.g. Matsunaga et al. 2009), the absorption-corrected flux of  $2.3 \times 10^{-12}$  erg cm<sup>-2</sup> s<sup>-1</sup> in the 2–10 keV band is converted to the source luminosity of  $1.8 \times 10^{34}$  erg s<sup>-1</sup> in the 2–10 keV band,

---

<sup>2</sup> <http://simbad.u-strasbg.fr/simbad/>

which places Suzaku J174035.6–301416 as the brightest class of the IP (Patterson 1994), and nearly the same order of faint neutron star binaries. However neutron star binaries do not exhibit strong Fe  $K\alpha$  line emissions and the EWs are typically less than 100 eV (Ng et al. 2010). Suzaku J174035.6–301416 might be one of the most powerful mCVs in the GC region. IPs are, however, well known to be intrinsically absorbed (e.g. Evans & Hellier 2007), and thus the measured absorption is not clear to be related to the interstellar absorption. Our estimation of the distance and luminosity should have large uncertainty. If we assume the luminosity of typical IPs,  $10^{31}$ – $10^{33}$  erg s $^{-1}$  (Ezuka & Ishida 1999), as that of Suzaku J174035.6–301416, the distance estimated to be 0.2–2 kpc from the observed flux.

#### 4.2. *Comments on the origin of HESS J1741–302 and the GCDX*

We find no excess X-rays from the southern emission peak region of HESS J1741–302 nor from the nearby radio pulsar PSR B1737–30. We constrain the flux ratio of TeV gamma to hard X-ray ( $F_{1-10\text{TeV}}/F_{2-10\text{keV}}$ ) to larger than  $\sim 12$ . Matsumoto et al. (2009) reported that X-ray emission is detected from the northern emission peak of HESS J1741–302 and  $F_{1-10\text{TeV}}/F_{2-10\text{keV}}$  is  $\sim 6$ . These large ratios may suggest that HESS J1741–302 is probably a ”dark accelerator” like HESS J1616–508 (Matsumoto et al. 2007). Unlike HESS J1745–303 (Bamba et al. 2009), we find no hint of the 6.4 keV line from the diffuse region of HESS J1741–30 or no possible correlation between the GCDX and TeV gamma-ray emission, at least for HESS J1741–302.

On the other hand, our discovery of an IP candidate may give new insight for the origin of GCDX. As we already note, significant fraction of the iron  $K\alpha$  lines in GCDX, would be due to mCVs. However the mean equivalent widths of the 6.4 keV and 6.7 keV lines in the GCDX are  $\sim 400$  eV and  $\sim 450$  eV, respectively (e.g. Koyama et al. 2009). These are significantly larger than those of Suzaku J174035.6–301416, and the other bright mCVs (Ezuka & Ishida 1999). This statement may be true for the most of the mCVs, which are bright enough to measure the iron lines. To solve this entangled issue, we need to measure the flux of iron  $K\alpha$  lines from fainter mCV and/or the other active stars.

The authors thank all of the Suzaku team members, especially T. Tsuru, M. Nobukawa, K. Makishima, T. Yuasa and M. Ishida for their comments and useful information on the XIS performance. This work is supported by the Grant-in-Aid for the Global COE Program ”The Next Generation of Physics, Spun from Universality and Emergence” and Challenging Exploratory Research (KK) from the Ministry of Education, Culture, Sports, Science and Technology (MEXT) of Japan. HU is supported by JSPS Research Fellowship for Young Scientists.

## References

- Aharonian, F., et al. 2006, *ApJ*, 636, 777
- Aharonian, F., et al. 2006, *Nature*, 439, 695
- Anders, E., & Grevesse, N. 1989, *Geochim. Cosmochim. Acta*, 53, 197
- Allan, A., Hellier, C., & Beardmore, A. 1998, *MNRAS*, 295, 167
- Bamba, A., Yamazaki, R., Kohri, K., Matsumoto, H., Wagner, S., Pühlhofer, G., & Kosack, K. 2009, *ApJ*, 691, 1854
- Cutri, R. M., et al. 2003, The IRSA 2MASS All-Sky Point Source Catalog, NASA/IPAC Infrared Science Archive. <http://irsa.ipac.caltech.edu/applications/Gator/>
- Evans, P. A., & Hellier, C. 2007, *ApJ*, 663, 1277
- Ezuka, H. & Ishida, M. 1999, *ApJS*, 120, 277
- Fomalont, E. B., Goss, W. M., Manchester, R. N., & Lyne, A. G. 1997, *MNRAS*, 286, 81
- Hog, E., Kuzmin, A., Bastian, U., Fabricius, C., Kuimov, K., Lindegren, L., Makarov, V. V., & Roeser, S. 1998, *A&A*, 335, L65
- Huovelin, J., Schultz, J., Vilhu, O., Hannikainen, D., Muhli, P., & Durouchoux, P. 1999, *A&A*, 349, L21
- Huovelin, J. Schultz, J, Vilhu, O., Hannikainen, D., Muhli, P., Durouchoux, P.2002, *arXiv:astro-ph/0208179*
- Ishida, M., Makishima, K., Mukai, K., & Masai, K. 1994, *MNRAS*, 266, 367
- Ishisaki, Y., et al. 2007, *PASJ*, 59, 113
- Kaastra, J. S., & Mewe, R. 1993, *A&AS*, 97, 443
- Koyama, K., et al. 2007a, *PASJ*, 59, S23
- Koyama, K., et al. 2007b, *PASJ*, 59, S245
- Koyama, K., Takikawa, Y., Hyodo, Y., Inui, T., Nobukawa, M., Matsumoto, H., Tsuru, T. 2009, *PASJ*, 61, S255
- Larsson, S. 1996, *A&AS*, 117, 197
- Matsumoto, H., et al. 2007, *PASJ*, 59, 199
- Matsumoto, H., Uchiyama, H., Tsuru, T., Koyama, K. & Tibolla, O. 2009, in the proceedings of The Energetic Cosmos: from Suzaku to Astro-H, 154
- Matsunaga, N., Kawadu, T., Nishiyama, S., Nagayama, T., Hatano, H., Tamura, M., Glass, I. S., & Nagata, T. 2009, *MNRAS*, 399, 1709
- Mitsuda, K., et al. 2007, *PASJ*, 59, S1
- Morrison, R. & McCammon, D. 1983, *ApJ*, 270, 119
- Muno, M. P., et al. 2003, *ApJ*, 589, 225
- Muno, M. P., et al. 2004, *ApJ*, 613, 326
- Muno, M. P., et al. 2009, *ApJS*, 181, 110
- Ng, C., Díaz Trigo, M., Cadolle Bel, M., & Migliari, S. 2010, *A&A*, 522, A96
- Nobukawa, M., Koyama, K., Matsumoto, H., & Tsuru, T. G. 2009, *PASJ*, 61, 93
- Norton, A. J., & Watson, M. G. 1989, *MNRAS*, 237, 853
- Ohnishi, T., Koyama, K., Tsuru, T., Masai, K., Yamaguchi, H. , Ozawa, M.2010, *PASJ*, submitted

- Revnivtsev, M., Lutovinov, A., Suleimanov, V., Sunyaev, R., & Zheleznyakov, V. 2004, *A&A*, 426, 253
- Parmar, A. N., Kuulkers, E., Oosterbroek, T., Barr, P., Much, R., Orr, A., Williams, O. R., & Winkler, C. 2003, *A&A*, 411, L421
- Patterson, J. 1994, *PASP*, 106, 209
- Prigozhin, G., Burke, B., Bautz, M., Kissel, S., Lamarr, B. 2008, *IEEE Transactions on Electron Devices*, 55, 2111
- Revnivtsev, M., Sazonov, S., Churazov, E., Forman, W., Vikhlinin, A., & Sunyaev, R. 2009, *Nature*, 458, 1142
- Ritter, H., & Kolb, U. 2003, *A&A*, 404, 301
- Ryu, S., Koyama, K., Nobukawa, M., Fukuoka, R., Tsuru, T. 2009, *PASJ*, 61, 751
- Sakano, M., Koyama, K., Murakami, H., Maeda, Y., & Yamauchi, S. 2002, *ApJS*, 138, 19
- Scaringi, S., et al. 2010, *MNRAS*, 401, 2207
- Serlemitsos, P., et al. 2007, *PASJ*, 59, S9
- Smith, R. K., Brickhouse, N. S., Liedahl, D. A., & Raymond, J. C. 2001, *ApJL*, 556, L91
- Tawa, N., et al. 2008, *PASJ*, 60, 11
- Tibolla, O., Komin, N., Kosack, K., & Naumann-Godo, M. 2009, *American Institute of Physics Conference Series*, 1085, 249
- Tibolla, O., et al. 2009, *Fermi Symposium*, Washington, D.C., Nov. 2–5; *eConf Proceedings C091122*
- Uchiyama, H., et al. 2009, *PASJ*, 61, S9
- Uchiyama, Y., et al. 2008, *PASJ*, 60, S35